Materials Science and Engineering A 533 (2012) 107–118

Contents lists available at SciVerse ScienceDirect

Materials Science and Engineering A

journal homepage: www.elsevier.com/locate/msea

Tensile properties of an AlCrCuNiFeCo high-entropy alloy in as-cast and wrought conditions

A.V. Kuznetsov[a,*], D.G. Shaysultanov[a], N.D. Stepanov[a], G.A. Salishchev[a], O.N. Senkov[b,c]

[a] Laboratory of Bulk Nanostructured Materials, Belgorod State University, Pobeda 85, Belgorod 308015, Russia
[b] Air Force Research Laboratory, Materials and Manufacturing Directorate, Wright-Patterson Air Force Base, OH 45433, USA
[c] UES, Inc., 4401 Dayton-Xenia Rd., Dayton, OH 45432, USA

ARTICLE INFO

Article history:
Received 30 September 2011
Received in revised form
19 November 2011
Accepted 21 November 2011
Available online 27 November 2011

Keywords:
Electron microscopy
Mechanical characterization
High entropy alloy
Thermomechanical processing
Grain refinement
Plasticity

ABSTRACT

Extensive multistep forging at 950 °C was applied to the cast AlCuCrFeNiCo high-entropy alloy to transform the cast coarse dendritic structure into a fine equiaxed duplex structure consisting of the mixture of BCC and FCC phases, with the average grain/particle size of ~1.5 ± 0.9 μm. Tensile properties of the alloy in the as-cast and forged conditions were determined in the temperature range of 20–1000 °C. The hot forged alloy was stronger and more ductile during testing at room temperature, than the as-cast alloy. The yield stress (YS), ultimate tensile strength (UTS), and tensile ductility (δ) of the forged condition were 1040 MPa, 1170 MPa, and 1%, respectively, against 790 MPa, 790 MPa and 0.2% for the as-cast condition. In both conditions, the alloy showed brittle to ductile transition (BDT), with a noticeable increase in the tensile ductility within a narrow temperature range. In the as-cast condition, this transition occurred between 700 and 800 °C, while in the forged condition, it was observed between 600 and 700 °C. With an increase in the testing temperature above the BDT, a continuous decrease in tensile flow stress and an increase in tensile ductility were observed. In the temperature range of 800–1000 °C, the forged alloy showed superplastic behavior. The tensile elongation was above 400% and reached 860% at 1000 °C.

1. Introduction

Modern technological developments and progress in engineering, particularly in the aerospace industry, require the development and utilization of new structural materials that would provide higher performance compared to the currently used structural materials. In the last decade, a new class of materials, so called high-entropy alloys (HEAs) was proposed and developed [1–3]. These alloys contain five to thirteen principal elements at equimolar or near-equimolar compositions, thus the atomic fractions of each element cannot be less than 5% and more than 35% [1]. The high entropy of mixing has been found to prevent formation of intermetallic phases and these alloys predominantly consist of a mixture of simple solid solutions and favorable combination of compression strength and ductility [1,4–13].

Many HEAs have high hardness, strength, wear resistance, and their microstructure is very stable against heat treatment [1,14,15]. This combination of properties is attractive for a wide range of applications; however, the main obstacle for using such materials is low ductility and brittleness of many HEAs, especially at room temperature. Annealing has been found to improve ductility of cast HEAs [9,16]. Due to their low ductility, almost all reported mechanical properties of high entropy alloys were obtained by compression testing or measuring hardness. Only several publications are yet available where tensile properties of HEAs are reported [10,17]. It is necessary to point out that almost all reported properties of HEAs were obtained in cast conditions and the properties of cast alloys are known to be almost always inferior to the properties of wrought alloys. Such structural constituents as shrinkage porosity, coarse dendritic structure, chemical heterogeneity, metastable eutectic at grain boundaries weaken mechanical properties of cast alloys. The microstructure and properties of castings can be improved by thermo-mechanical treatment, including extensive hot working [18–22]. Unfortunately, no publications have yet been available in the open literature on the effect of hot working processes on the properties of HEAs.

In this paper, microstructure and tensile properties of a severe plastically deformed AlCrCuNiFeCo high entropy alloy are presented and compared with those of the cast alloy. This alloy was selected for study because it has been most widely studied among all other HEAs [1,9,23–25] and the approximate phase diagram has been reported [24], which allowed selection of the temperature range for the thermomechanical treatment.

* Corresponding author. Tel.: +7 4722 585416; fax: +7 3472 585415.
E-mail addresses: kuznetsov@bsu.edu.ru, ak72@mail.ru (A.V. Kuznetsov).

0921-5093/$ – see front matter © 2011 Elsevier B.V. All rights reserved.
doi:10.1016/j.msea.2011.11.045

Table 1
Chemical composition of the studied alloy.

	Al	Cr	Cu	Ni	Fe	Co
Atomic %	16.16 ± 0.63	15.86 ± 0.05	17.42 ± 0.01	16.65 ± 0.23	15.96 ± 0.15	17.07 ± 0.19
Weight %	8.20 ± 0.40	15.65 ± 0.05	20.95 ± 0.05	18.55 ± 0.25	17.80 ± 0.10	18.10 ± 0.20

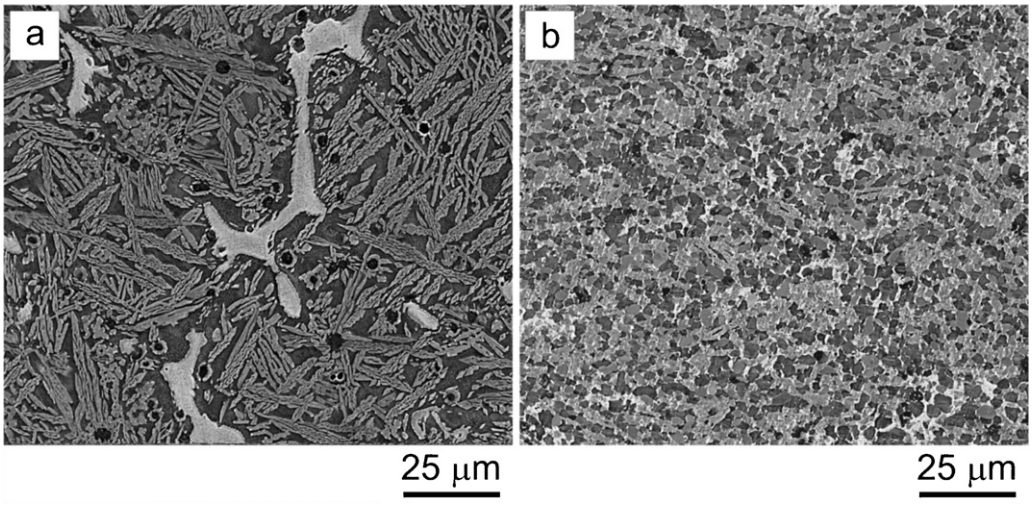

Fig. 1. Microstructure of the AlCrCuNiFeCo HEA in (a) as-cast and (b) hot forged conditions.

2. Experimental procedures

A 40 mm in diameter and 90 mm in height cylindrical ingot of the AlCrCuNiFeCo high-entropy alloy was produced by induction melting of the constituent elements followed by electro-slag re-melting and casting into a water-cooled copper mold. The chemical composition of the ingot is given in Table 1. Two slices, about 10 mm thick, were cut-out from the top and bottom of the cast ingot, and a blank of 40 mm in diameter and 35 mm long was extracted from the remaining part. This blank was homogenized by holding for 50 h at 960 °C. After homogenization, the blank was extensively hot worked at 950 °C using multistep *a*–*b*–*c* forging in three orthogonal directions [20–22]. A hydraulic press DEVR 4000 with the maximum force of 0.4 MN, equipped with a radial furnace, was used for the isothermal forging. The ram speed was 1 mm/s and the total true strain achieved during forging was ~1000%.

Microstructure of cast and deformed samples was studied on polished cross-sections using scanning electron microscopes Quanta 200-3D and Quanta 600 equipped with backscatter electron detector, as well as with energy dispersive spectroscopy (EDS) and electron backscatter diffraction (EBSD) detectors. Vickers microhardness, HV, was measured on polished cross-section surfaces using a 136° Vickers diamond pyramid under a 250 g load applied for 15 s. Uniaxial tensile tests were conducted in air using an Instron 5882 testing machine equipped with a furnace for heating up to 1200 °C. The testing was conducted at temperatures in the range of 20–1000 °C, and a ram speed of 0.016 mm/s (initial strain rate of 10^{-3} s^{-1}) was used. The tensile samples had the gauge length of 16 mm and a rectangular gauge cross-section of 3 mm × 1.5 mm.

3. Results and discussion

3.1. Effect of multi-step forging on microstructure

The dendritic microstructure of the as-cast alloy is shown in Fig. 1a. The dendrite size is about 50 μm. According to the EBSD analysis, the microstructure consists of a BCC matrix (dark regions, the volume fraction is ~53%) and FCC particles (lighter regions, the volume fraction is ~47%). The FCC particles located at grain boundaries (i.e. inter-dendritic regions) are larger and brighter than the gray particles located inside the BCC grains (dendrites). Chemical analysis by EDS shows that the inter-dendritic FCC particles have much larger amount of Cu than the intra-dendritic FCC particles. X-ray diffraction analysis of the as-cast sample reveals the presence of a BCC and two FCC phases, Fig. 2a, with the lattice parameters a = 2.88 Å (BCC), 3.60 Å (FCC1) and 3.63 Å (FCC2).

Considerable refinement of the cast microstructure occurs after extensive multi-step forging at 950 °C (Fig. 1b). The non-homogeneous dendritic structure typical to the as-cast condition transforms to a recrystallized, duplex-type structure. The BCC grains become fine and equiaxed, whereas the FCC particles are refined, have near-equiaxed shape and are homogeneously distributed in the forged samples. According to the EBSD analysis, the volume fraction of the BCC phase after forging increases to ~60% and the FCC phase decreases to ~40%. The X-ray diffraction pattern from the forged sample, shown in Fig. 2b, reveals that in addition to the BCC and two FCC phases, which lattice parameters are

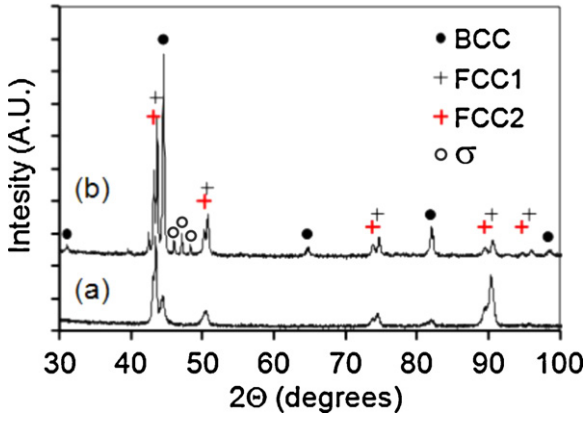

Fig. 2. X-ray diffraction pattern of the AlCuCrFeNiCo alloy in (a) as-cast and (b) forged conditions.

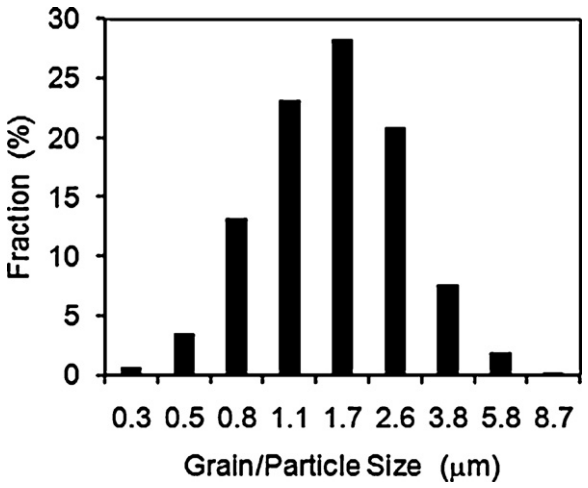

Fig. 3. Grain/particle size distribution in the AlCuCrFENiCo alloy after hot forging at 950 °C with the total true strain $e = 10$. Note the logarithmic scale of X-axis.

similar to those in the as-cast condition, a σ phase (enriched with Cr and Fe) is also present in the forged alloy. Characteristic small-intensity peaks from the σ phase are located between (1 1 1) and (2 0 0) peaks of the FCC phases. These peaks are absent in the as-cast condition. The duplex microstructure of the forged alloy is characterized by a lognormal distribution of grain/particles sizes, Fig. 3, and the average grain/particle size is estimated to be 1.5 ± 0.9 μm along the cross-section of the forged material. The high value of the standard deviation ($s = 0.9$ μm) is due to large variations of the grain/particle sizes (from 0.2 to 6.1 μm) in the microstructure.

3.2. Mechanical properties

Fig. 4 shows typical tensile behavior at $\dot{\varepsilon} = 10^{-3}\ s^{-1}$ and different temperatures of (a) as-cast and (b) hot forged samples of the studied alloy. The values of the yield stress (YS), $\sigma_{0.2}$, ultimate tensile stress (UTS), σ_u, and elongation to fracture, δ, of these samples at different temperatures are given in Table 2. At room temperature, the as-cast alloy is brittle and it fractures immediately after yielding, so that YS and UTS have the same values of 790 MPa and the fracture strain $\delta = 0.2\%$. After hot forging, the alloy becomes stronger and shows some ductility at room temperature. Namely, its YS = 1040 MPa, UTS = 1170 MPa and $\delta = 1.0\%$.

A noticeable increase in the tensile ductility of the cast alloy (from ~4.7% to 12.1%) occurs in the temperature range of 700–800 °C, which is likely caused by the brittle-to-ductile transition (BDT). This increase in tensile ductility is accompanied with a noticeable decrease in tensile strength. For example, YS decreases from 350 MPa to 161 MPa and UTS decreases from 360 MPa to 180 MPa with an increase in temperature from 700 °C to 800 °C (see Fig. 4a and Table 2). A further increase in testing temperature to 1000 °C results in a continuous decrease in YS to 37 MPa and UTS to 44 MPa, and an increase in tensile ductility of the cast alloy to $\delta = 77\%$. Analysis of the deformation curves of the cast alloy samples (Fig. 4a) shows that in the temperature range 700–1000 °C a peak stress is achieved shortly after yielding followed by an apparent decrease in tensile stress with further deformation. The total elongation is mainly controlled by the duration of this strain-softening stage. The apparent decrease in tensile stress after reaching the peak stress is likely due to strain localization and neck formation. One may therefore suggest that the increase in the duration of the softening stage is due to slowing down the neck development with an increase in temperature.

The forged alloy shows a strong BDT behavior, with a rapid increase in tensile ductility from 1.3% to 63%, in the temperature range of 600–700 °C (see Fig. 4b and Table 2), i.e. at a lower temperature than the as-cast alloy. The associated drop in the YS (from 300 MPa to 63 MPa) and UTS (from 350 MPa to 91 MPa) is much more rapid than that of the cast alloy. At temperatures above the BDT, the forged alloy is considerably softer and much more deformable than the cast alloy. For example, at $T = 800$ °C, the UTS

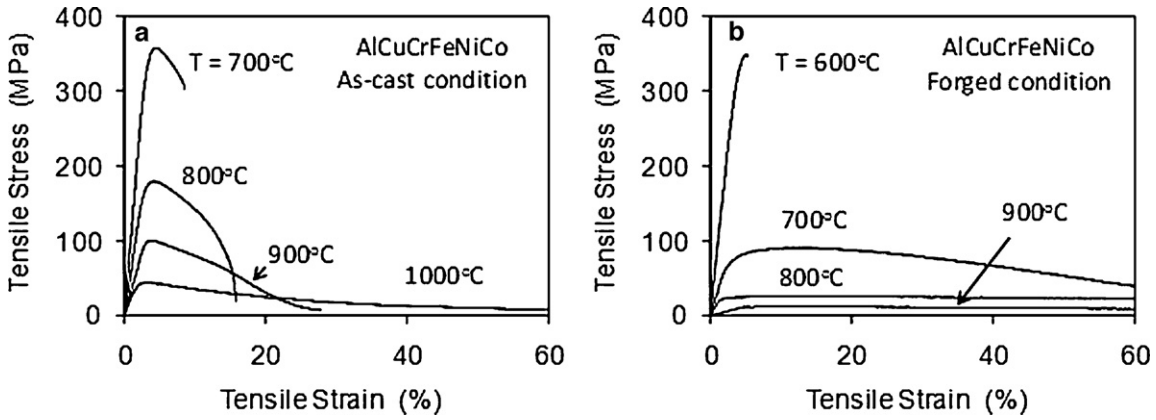

Fig. 4. Typical stress–strain curves of the as-cast (a) and hot forged (b) samples deformed at different temperatures and the initial strain rate of $10^{-3}\ s^{-1}$.

Table 2
Tensile properties of the AlCrCuNiFeCo alloy samples in as-cast condition and after multistep forging.

Temperature condition	20 °C	300 °C	600 °C	700 °C	800 °C	900 °C	1000 °C
As-cast							
$\sigma_{0.2}$, MPa	790	–	542	350	161	88	37
σ_u, MPa	790	–	551	360	180	100	44
δ, %	0.2	–	0.4	4.7	12.1	30	77
Forged							
$\sigma_{0.2}$, MPa	1040	810	300	63	22	14	9
σ_u, MPa	1170	880	350	91	26	18	22
δ, %	1.0	0.4	1.3	63	604	405	864

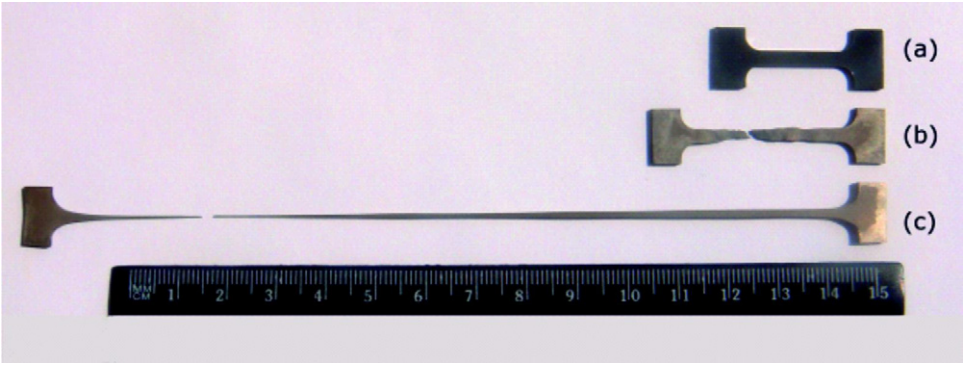

Fig. 5. Photographs of tensile samples after deformation at 1000 °C: (a) a non-deformed sample; (b) as-cast sample (δ = 77%); and (c) forged sample (δ = 864%). $\dot{\varepsilon} = 10^{-3}\ s^{-1}$.

of the alloy in as-cast condition ($\sigma_u^{cast} = 180$ MPa) is more than 6 times higher than in the forged condition ($\sigma_u^{forge} = 26$ MPa) and even at T = 1000 °C the cast condition is ~3 times stronger than the forged condition ($\sigma_u^{cast} = 44$ MPa and $\sigma_u^{forge} = 14$ MPa). It is interesting to note that the BDT in the cast and forged alloys occurs at almost the same UTS values of ~350 MPa and thus the shift of the BDT temperature of the forged alloy towards lower temperature range can be associated with the stronger temperature dependence of the UTS of the forged alloy. The forged samples exhibit steady-state flow and very high elongation at temperatures above BDT, which reaches 604% at 800 °C and 864% at 1000 °C (Fig. 4b and Table 2). Fig. 5 shows photographs of as-cast and forged samples after tensile deformation at 1000 °C. Though the cast sample illustrates pronounced strain localization (necking) and final fracture by shear at δ = 77%, the forged sample shows very homogeneous flow, high resistance to neck formation, and very high elongation of δ = 864%. It is expected that very high elongation and low flow stress of the forged alloy is an indication of superplastic behavior at T = 800–1000 °C.

The Vickers microhardness of the tensile samples tested at different temperatures is tabulated in Table 3. Microhardness of the as-cast samples is always higher than that of the forged samples. Microhardness of slightly deformed neck regions (at 20 °C, 600 °C and 700 °C) is almost the same as the microhardness of non-deformed head regions. On the other hand, severely deformed neck regions of the forged samples (700–1000 °C) and as-cast samples (1000 °C) have noticeably smaller microhardness than the head regions of the respective samples, which is due to development of porosity in the highly deformed regions (see below). A noticeable increase in microhardness can be seen in the as-cast specimen after holding and tensile deformation at 800 °C, which is probably due to aging associated with phase transformations (σ-phase precipitation) in this temperature range [10].

3.3. Microstructure evolution during tensile deformation

SEM backscatter images of the microstructure of the non-deformed (head) and deformed (gauge-neck) regions of the tensile samples of the as-cast alloy after deformation at 700 °C, 800 °C, 900 °C and 1000 °C are shown in Fig. 6. Different outlook of the FCC particles inside dendrites in different samples is probably due to their plate-like morphology and different orientation of dendritic grains. No noticeable changes in the dendritic microstructure of the as-cast condition are identified after deformation at 700 °C and 800 °C: the microstructure remains similar to that of the as-cast alloy in both head and neck regions (Fig. 6a–d). During deformation at 900 °C, fragmentation and globularization of coarse FCC particles are observed in the gauge region, while no noticeable changes are detected in the head (non-deformed) region (Fig. 6e and f). After deformation at 1000 °C, the microstructure in the gauge region completely transforms into a recrystallized duplex grain structure with homogeneously distributed near-equiaxed FCC particles (Fig. 6h). The average particle size (BCC and FCC) is ~2.4 ± 1.0 μm. It is worth noting that holding of the sample at 1000 °C for the same time, but without deformation, does not lead to any noticeable visual changes in the cast dendritic structure, at least at the used magnifications (compare Fig. 1a and Fig. 6g).

Tensile deformation in the temperature range from 20 °C to 1000 °C of the forged alloy samples does not change the morphology of the forged microstructure (Fig. 7). However, grain/particle coarsening is noted after deformation at 900 °C and 1000 °C. For example, the average grain/particle size in non-deformed (head) region increases from 1.5 μm (as-forged condition) to 2.5 μm after deformation at 900 °C and to 2.8 μm after deformation at 1000 °C. The grain/particle size in the heavily deformed neck region is slightly smaller (i.e. 2.2 μm at 900 °C and 2.6 μm at 1000 °C) than in the non-deformed region of respective specimens (see Table 4), which may indicate some deformation-induced particle fragmentation.

3.4. Porosity development in tensile tested samples

The as-cast samples deformed by tension in the temperature range of 20–700 °C do not show any porosity in the deformed region (Fig. 8a). Fracture of these samples occurs by crack propagation, mainly along inter-dendritic regions. After tensile deformation at 800 °C and 900 °C of the as-cast samples, cracks developed at the interfaces of the FCC/BCC particles tend to blunt and transform to pores due to plastic deformation of surrounding areas (Fig. 8c and e). The cracks leading to fracture propagate along the interfaces, which are ~45° to the tensile direction. The pore morphology of the as-cast sample deformed at 1000 °C (δ = 77%) is different from the described above. At this temperature, the pores are elongated in the tensile direction due to heavy deformation of surrounding matrix and fracture occurs by local necking and thinning of inter-pore areas (Fig. 8g).

Tensile deformation at T > 600 °C of the initially forged alloy samples results in a considerable amount of pores and cracks inside wide area under the fracture surface (Fig. 8b, d, f and h). While at 700 °C the pores are formed and developed along interfaces of the FCC particles, which are nearly perpendicular to the tension direction, and thus form chains in the radial directions (Fig. 8b), at higher temperatures the pores are elongated in the longitudinal direction (Fig. 8d, f and h). Superplastic-like behavior in this temperature range (800–1000 °C) resists strain localization and necking between the nearest elongated pores and results in formation of very long pores. A detailed analysis of the microstructure of these samples shows that, similar to the as-cast condition, the

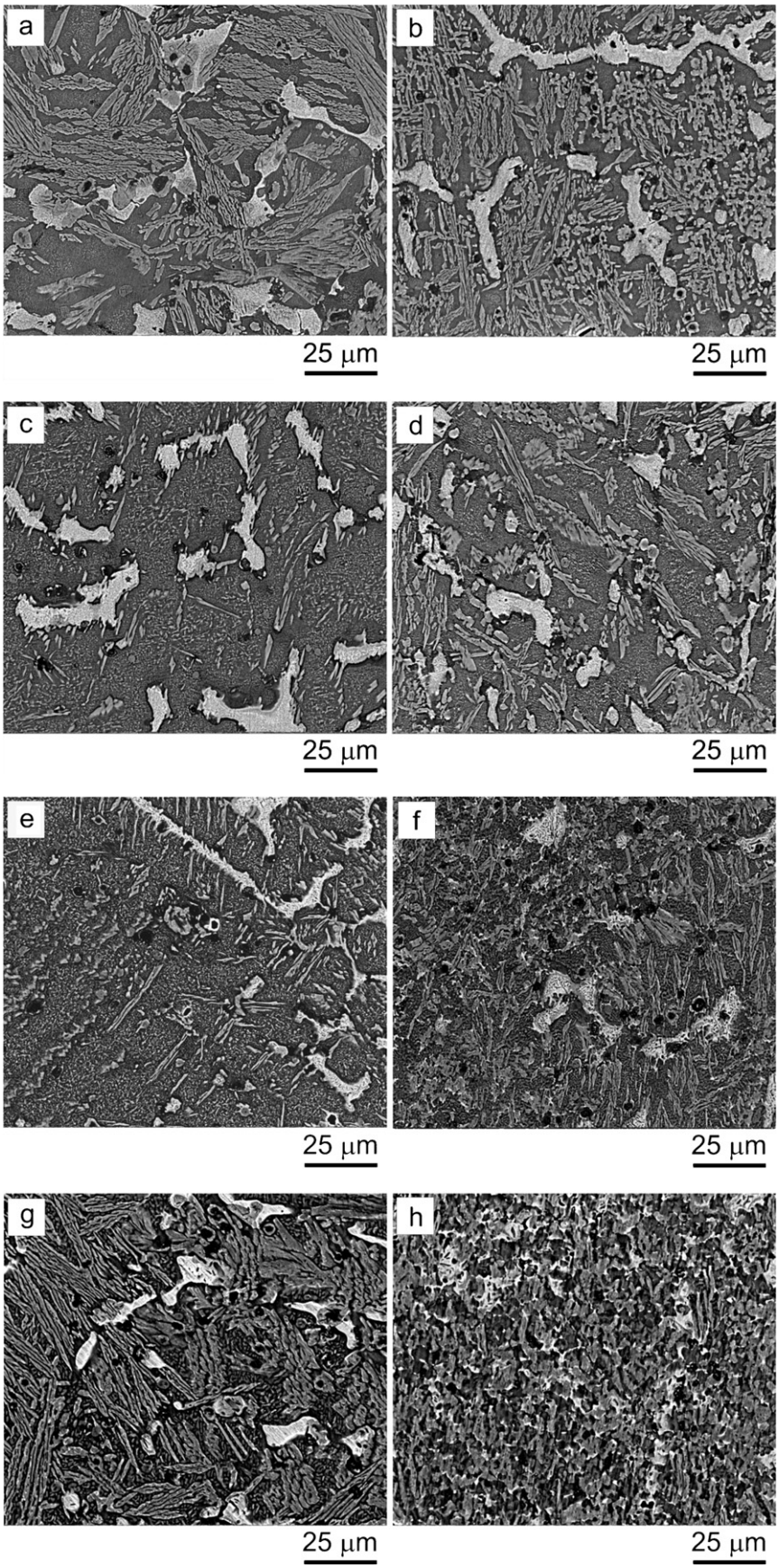

Fig. 6. Microstructure of the as-cast AlCuCrFeNiCo alloy after tensile testing at (a and b) 700 °C; (c and d) 800 °C; (e and f) 900 °C; (g and h) 1000 °C; (a, c, e and g) non-deformed (sample head) regions and (b, d, f and h) deformed (gauge-neck) regions.

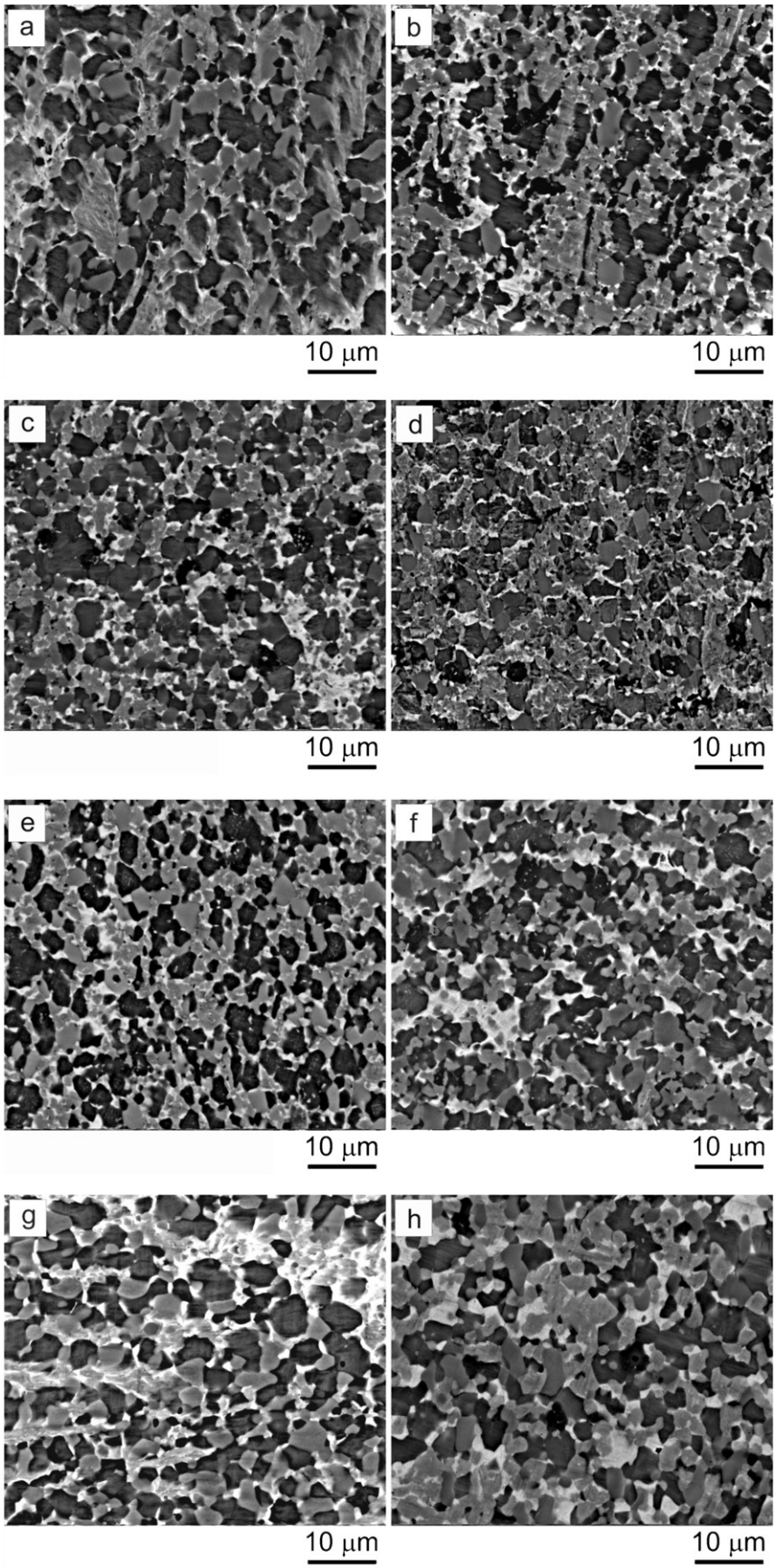

Fig. 7. Microstructure of the forged alloy samples after tensile deformation to fracture at temperatures (a and b) 600 °C; (c and d) 700 °C; (e and f) 800 °C; (g and h) 900 °C; (i and j) 1000 °C; (a, c, e, g and i) non-deformed (head) regions and (b, d, f, h and j) deformed (gauge-neck) regions.

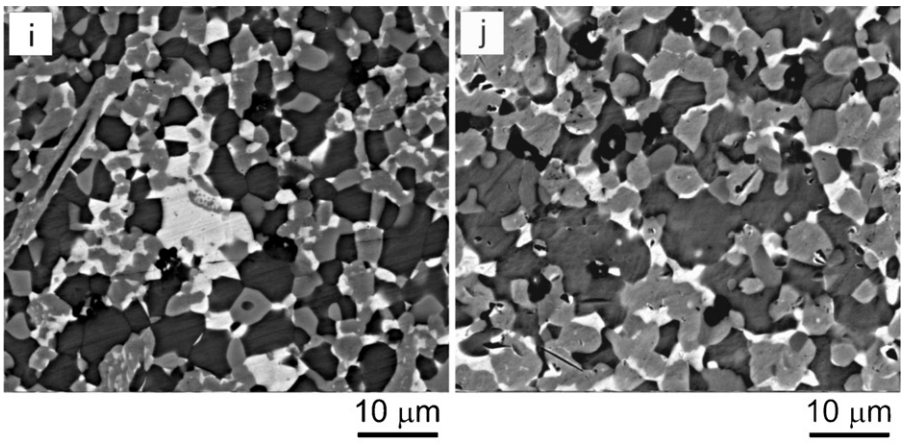

Fig. 7. (*Continued*).

pores and cracks are initiated at the interfaces between BCC and FCC phases.

Fig. 9a shows the temperature dependence of the volume fraction of pores in the neck regions of the as-cast and forged samples after tensile testing to fracture. With an increase in the testing temperature from 700 °C to 1000 °C the amount of neck porosity increases from 0.1% to 1.0% in the cast samples. At the same time, the neck porosity in the forged samples rapidly increases from 0.2% at 600 °C to 10.5% at 700 °C, reaches the maximum value of 12.5% at 900 °C and then decreases to 7.9% at 1000 °C. The high amount of porosity in the neck region of the forged samples is mainly associated with high tensile deformation of these samples at T = 800–1000 °C. To take this into account, the volume fractions of pores are normalized to the respective total strains, and the results are given in Fig. 9b. The volume fraction of pores developed per 1% elongation is almost temperature independent for the cast material and is ~0.01–0.02%. At the same time, the volume fraction of pores developed per 1% elongation in the forged samples has maximum of 0.17% at 700 °C, rapidly decreases to ~0.02–0.03% at 800 °C and remains almost independent on temperature (within the experimental error) in the range of 800–1000 °C.

3.5. Fractography

The SEM images of fracture surfaces of the cast and forged samples tensile tested at 20 °C are shown in Fig. 10a–d, respectively. At low magnification, the as-cast alloy sample has a coarse faceted appearance of the fracture surface (Fig. 10a), whereas the forged sample has fine granular appearance of the fracture surface (Fig. 10c). This observation is consistent with the much smaller grain/particle size of the forged condition than the cast condition. Higher magnification images confirm brittle, quazi-cleavage, fracture of the as-cast alloy, with such characteristic features as flat facets, angular faceted steps, river-pattern markings, cleavage feathers and tongues (Fig. 10b). At the same time, higher magnification images from the fracture surface of the forged sample confirm mixed type of brittle and ductile fracture (Fig. 10d). The brittle type fracture is reflected by the presence of flat facets with characteristic river-pattern markings inside large dimples, while the ductile type fracture is reflected in numerous dimples of different diameters surrounding the flat facets. It is likely that during tensile deformation of the forged sample, cracks are formed at the interfaces of the BCC and FCC particles by brittle fracture and then the crack opening into voids occurs by plastic deformation of nearest, more ductile regions, as it is seen in Fig. 8b.

SEM images of the fracture surfaces of the as-cast alloy samples after tensile fracture in the BDT range at 700 °C and 800 °C are shown in Fig. 11a–d, respectively. Fracture at 700 °C (beginning of the BDT) is somewhat similar to fracture at 20 °C [compare Fig. 11a and b and Fig. 10a and b] in a sense that the quazi-cleavage facets dominate. However, the microstructure features, such as angular faceted steps, river-pattern markings and cleavage feathers, are finer at 700 °C, which is indirect indication of dislocation activity in the cleaved BCC phase before fracture. Indeed, the angular faceted steps are generally associated with crossing dislocation walls consisting of screw dislocations; thus higher number density of these steps indicates an increased number density of screw dislocations in the samples deformed at 700 °C than in the samples deformed at 20 °C. Additionally, the presence of plastically formed hills and

Table 3
Vickers microhardness of as-cast and forged AlCrCuNiFeCo alloy samples after tensile testing at different temperatures.

Testing temperature (°C)	20	600	700	800	900	1000
As-cast condition						
Head	463 ± 12.7	–	433 ± 17.6	472 ± 15.6	469 ± 15.3	405 ± 9.5
Neck	439 ± 14.1	–	449 ± 15.3	498 ± 20.6	445 ± 33.3	372 ± 26.9
Forged condition						
Head	432 ± 3.4	432 ± 11.4	410 ± 2.1	419 ± 2. 7	418 ± 3.4	392 ± 2.1
Neck	420 ± 2.6	435 ± 13.4	332 ± 5.7	349 ± 5.3	334 ± 4.9	388 ± 5.7

Table 4
The average particle size and standard deviation (in μm) in the duplex structure of the forged AlCrCuNiFeCo alloy samples after tensile deformation at given temperatures.

Testing temperature (°C)	600	700	800	900	1000
Particle size (μm) non-deformed (head) region	1.5 ± 0.8	1.6 ± 0.9	1.9 ± 1.0	2.5 ± 1.3	2.8 ± 1.3
Deformed (neck) region	1.6 ± 0.8	1.5 ± 0.8	1.6 ± 0.9	2.2 ± 1.1	2.6 ± 1.4

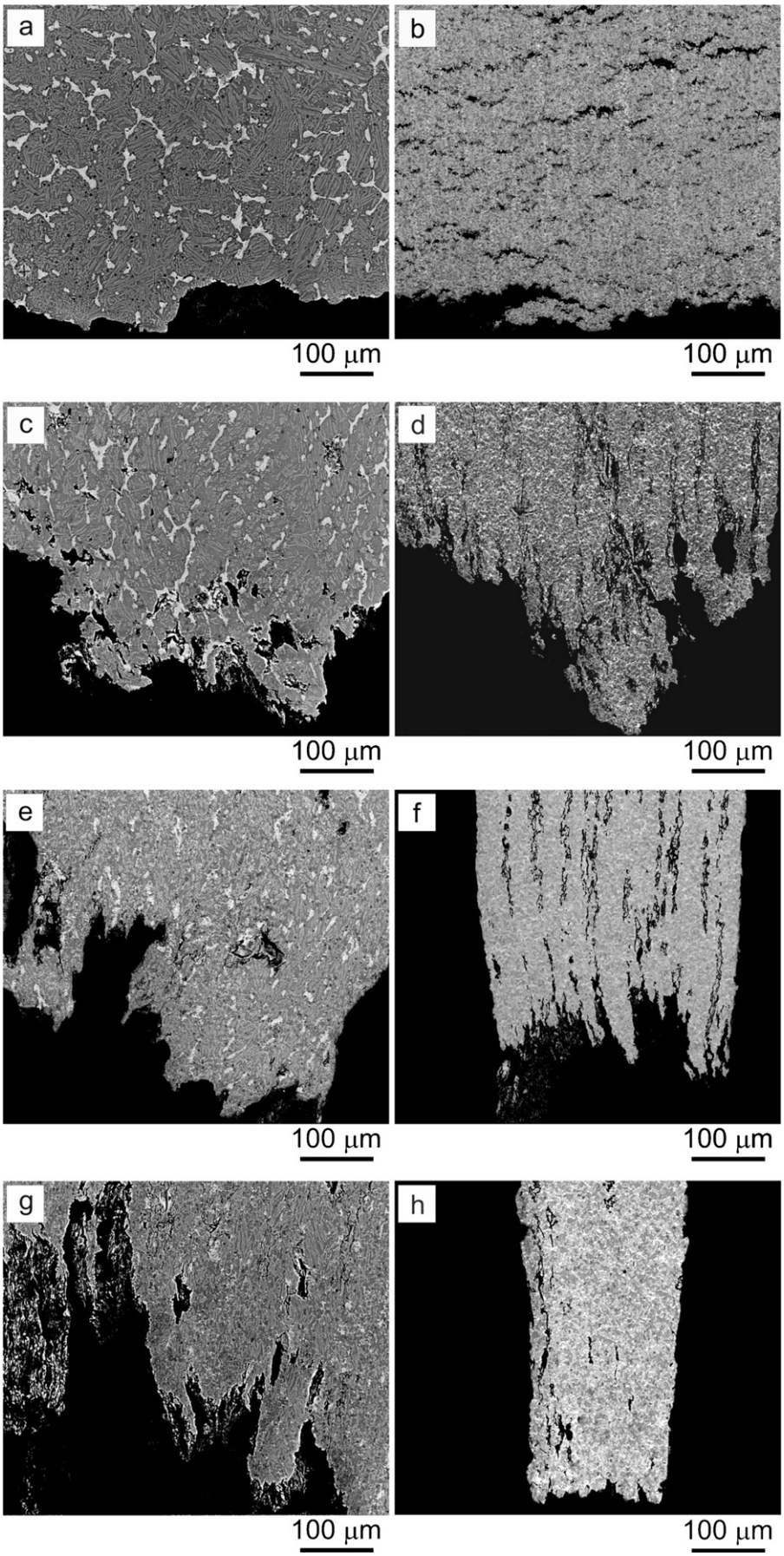

Fig. 8. Microstructure of the neck regions of the (a, c, e and g) as-cast and (b, d, f and h) forged alloy samples after tensile deformation to fracture at temperatures: (a and b) 700 °C; (c and d) 800 °C; (e and f) 900 °C; (g and h) 1000 °C.

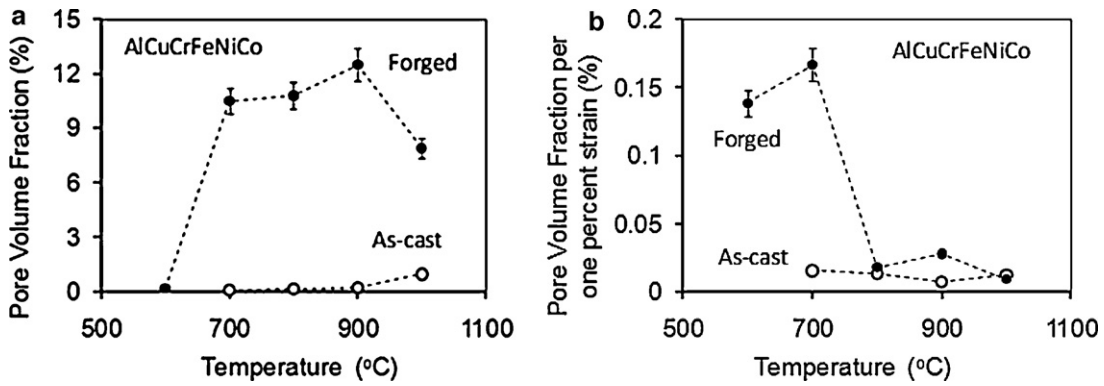

Fig. 9. (a) Volume percent of pores in the neck region of the samples after tensile deformation to fracture as a function of the testing temperature and (b) the same data normalized to the total elongation (% pores per 1% elongation) ($\dot{\varepsilon} = 10^{-3}\ s^{-1}$).

dimples is an indication of a ductile-type fracture mode in the as-cast alloy sample after deformation at 700 °C.

Fractographs of the as-cast alloy sample after tensile fracture at 800 °C are very different from described above. First, large pores developed during plastic deformation are seen at low magnification (Fig. 11c). Many of these pores are connected with secondary cracks and form chains. Second, the size and fraction of quazi-cleavage facets considerably decrease and new fine features of globular appearance are now present in the fracture surface (Fig. 11c and d). These fine globules can form during heavy local plastic deformation and dynamic recrystallization of the near-fracture region of the deformed sample. Indeed, the sample cross-section in this region is estimated by SEM to be ~1.0 mm × 2.2 mm, which results in the local plastic strain of ~200%, i.e. much higher than the total elongation of 12.1%. Oxidation of thin edges of ductile dimples, hills and tongues during holding at 800 °C can also led to

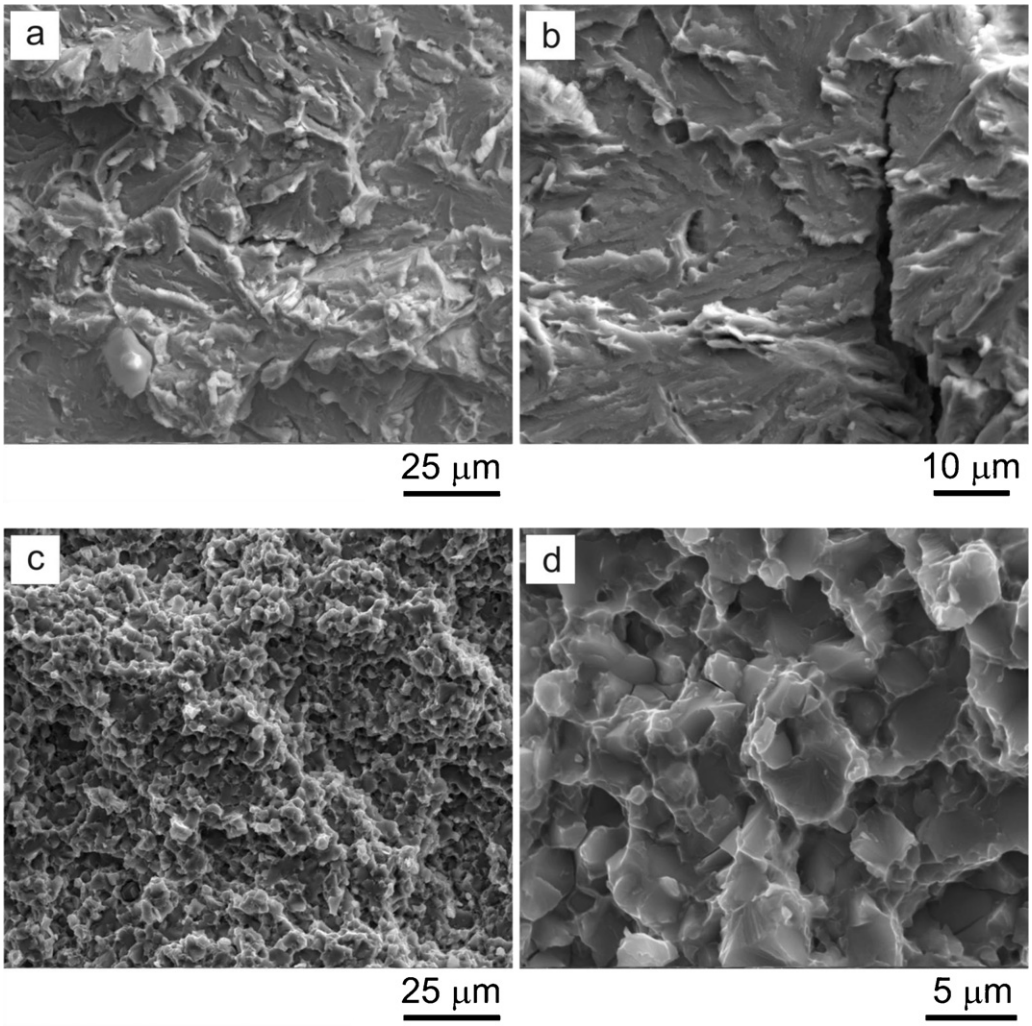

Fig. 10. SEM images of the fracture surfaces of tensile samples after tensile testing deformation at room temperature: (a and b) as-cast and (c and d) hot forged conditions.

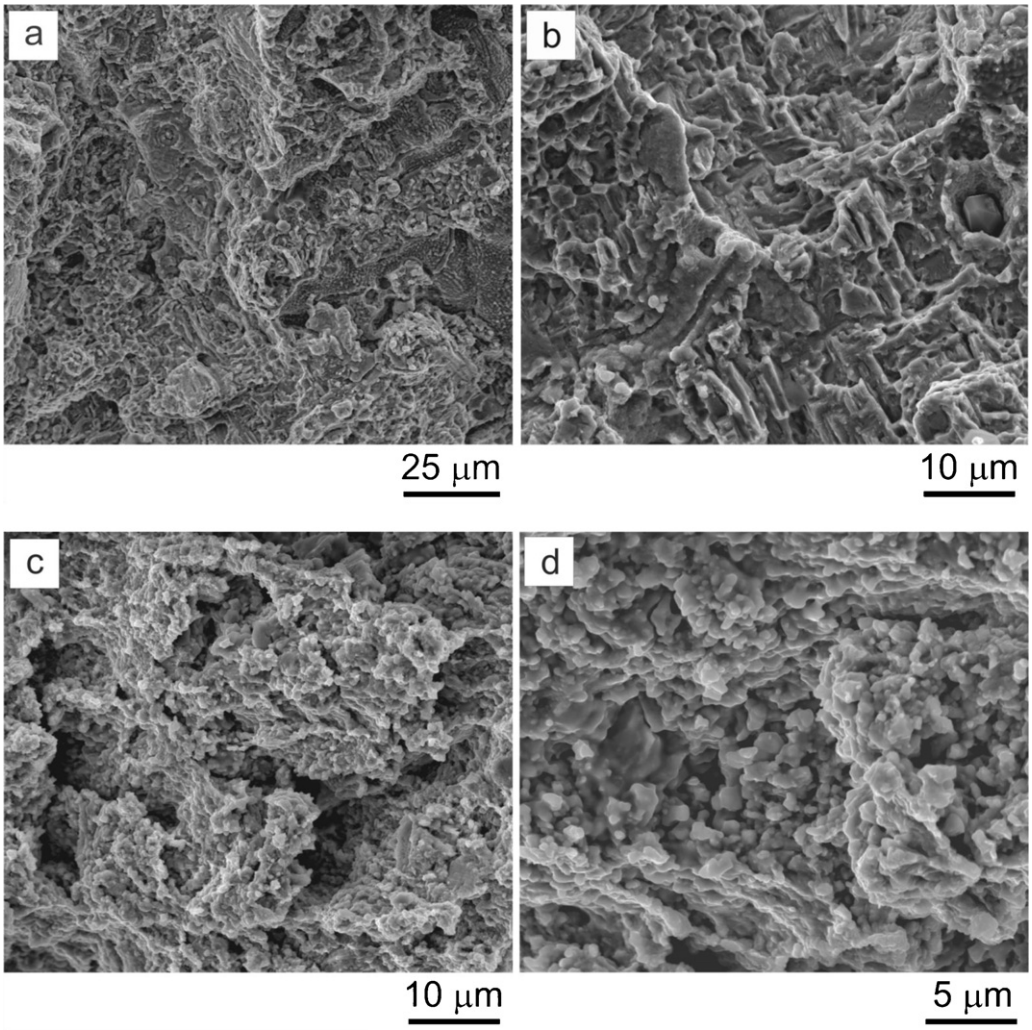

Fig. 11. SEM images of the fracture surfaces of the as-cast samples after tensile testing to fracture at (a and b) 700 °C and (c and d) 800 °C.

fragmentation and formation of oxidized globules in these regions. The blunt appearance of the fracture surface features is an indication of the surface oxidation.

Fig. 12 illustrates SEM images of fracture surfaces of the forged alloy samples, which were tensile fractured at 600 °C (a) and 700 °C (b). The fracture morphology at 600 °C (below BDT) is completely identical to that at 20 °C (compare with Fig. 10d). Namely, mixed type of brittle and ductile fracture is clearly seen. Similar to 20 °C sample, the brittle type fracture is reflected by the presence of flat facets with characteristic river-pattern markings inside large dimples, while the ductile type fracture is reflected in numerous dimples of different diameters surrounding the flat facets. The facture at 700 °C (above BDT) shows mainly ductile fracture with large dimples 2–5 μm in size. This finding is consistent with growth of the experienced total elongation up to 63%.

4. Discussion

Results described in previous sections demonstrate that hot working by multi-step forging of the AlCrCuNiFeCo high entropy alloy considerably modifies and refines the microstructure of the cast condition, improves tensile ductility and strength at room temperature, decreases brittle-to-ductile transition temperature by ~100 °C, and makes the alloy superplastic in the temperature range of 800–1000 °C.

4.1. Effect of hot deformation on microstructure

Thermomechanical processing is known to be an effective method and is widely used for the homogenization and modification of the coarse dendritic structure of cast metallic materials aiming at improving mechanical properties [19–22]. The current work shows that it can also be successfully applied to multi-component high entropy alloys. In particular, the cast ingot of the AlCrCuNiFeCo alloy was extensively hot worked by multi-step forging at 950 °C without any evidence of cracking, and a coarse dendritic structure of casting (the dendrite size is 50 μm) was completely transformed into a fine-grained duplex mixture of the BCC matrix and FCC particles, with an average grain/particle size of 1.5 μm and the relative volume fraction of the BCC and FCC phases of ~60% and ~40%, respectively. Small amount of a complex σ phase was also identified in the forged alloy.

4.2. Effect of microstructure on tensile properties

The refined microstructure of the hot forged material improves strength and ductility at room temperature as compared to the

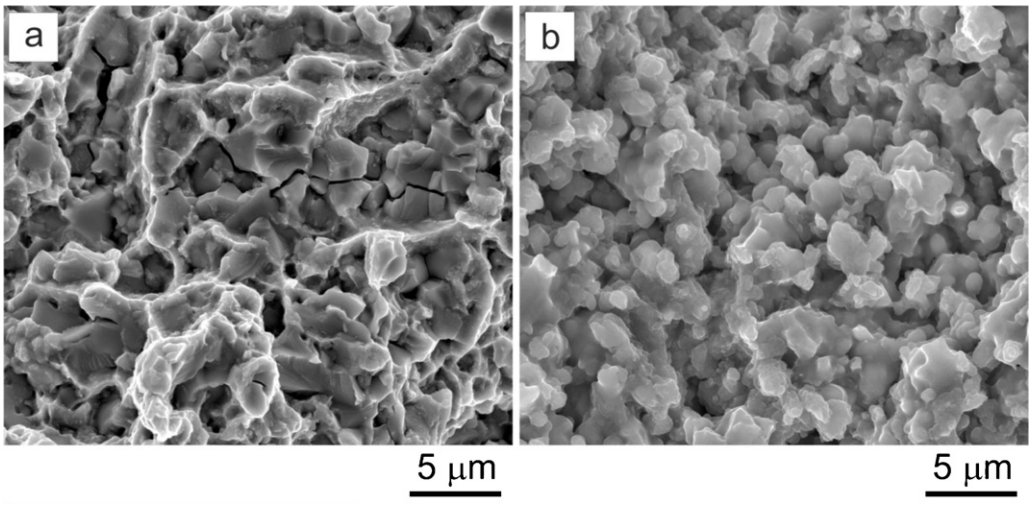

Fig. 12. SEM images of the fracture surfaces of hot forged samples after tensile testing to fracture at (a) 600 °C and (b) 700 °C.

initial cast condition. This is apparently due to grain refinement, which is known to effectively reduce strain localization and local stress concentrations at grain boundaries [26]. Elementary cracks associated with trans-granular brittle fracture are smaller and more work is required to propagate them in a critical-size crack to break the forged alloy with a refined grain structure than the coarse-grained as-cast alloy, thus explaining increased fracture strength and improved ductility. The alloy in both as-cast and forged conditions shows an obvious BDT, which is likely due to the presence of the high volume fraction (~60%) of the BCC phase. Presence of the ductile fracture mode in addition to the major brittle fracture mode in the samples fractured below BDT indicates that the brittle fracture in this alloy is preceded by local plastic deformation, probably in more ductile FCC phase. This plastic deformation is more extensive in the fine-grained forged condition than in the coarse-grained cast condition. Grain refinement by hot forging reduces the BDT temperature by about 100 °C in comparison with the as-cast condition. At the same time, the BDT is noted to start at almost the same UTS value of ~350 MPa in both microstructural conditions. These observations clearly indicate that the shift of the BDT towards lower temperatures is associated with a stronger temperature dependence of the YS and UTS and, therefore, more rapid decrease in the resistance to dislocation motion and stress relaxation with an increase in temperature in the forged alloy than in the as-cast alloy. Indeed, the forged alloy has higher area density of grain boundaries and interfaces than the as-cast alloy, and the grain boundary areas generally soften much faster with an increase in temperature towards the equicohesive temperature than trans-granular regions [27].

A noticeable increase in ductility and decrease in tensile strength observed at temperatures above the BDT are probably due to activation of grain boundary sliding (GBS) accommodated by diffusion-controlled processes. A more pronounced drop in the tensile strength and an increase in the tensile ductility in the forged alloy are again associated with finer grain structure, resulting in a more extensive GBS and dynamic recovery. Moreover, GBS-controlled plastic deformation is characterized by high strain rate sensitivity of the flow stress, which resists strain localization and neck formation and promotes superplastic deformation [22,28,29]. Such superplastic behavior results in the very long steady-state plastic flow of the forged alloy in the temperature range of 800–1000 °C. On the other hand, higher resistance to plastic deformation of the cast dendritic structure produces conditions for initiation of dynamic recrystallization, which refines the grain structure in heavy deformed regions of the cast samples at 800–1000 °C.

5. Conclusion

1. Extensive hot working by multi-step forging considerably refined the dendritic structure of the cast AlCuCrFeNiCo alloy and led to formation of fine equiaxed duplex structure with the grain/particle size of ~1.5 μm.
2. At room temperature, the AlCuCrFeNiCo alloy was stronger and more ductile after hot working than in as-cast condition. For example, in as cast condition the ultimate tensile strength (UTS) was 790 MPa and the alloy fractured at yielding (~0.2% plastic strain). At the same time, after hot working, the ultimate tensile strength increased to 1170 MPa and the tensile fracture occurred after 1% plastic strain.
3. In both as-cast and hot working conditions, the alloy shows brittle to ductile transition (BDT), with a considerable increase in the tensile ductility within a narrow temperature range. In the as-cast condition, this transition occurred when the testing temperature reached 700–800 °C range, while in the hot worked condition, it was observed in the 600–700 °C range. In both conditions, the UTS decreased with an increase in temperature and the BDT occurred when the UTS values drop to ~350 MPa. The decrease in the BDT temperature was explained by grain/particle refinement during hot working.
4. At temperatures above the BDT temperature, a considerable decrease in the tensile flow stress was observed. For example the UTS of as-cast alloy decreased from 350 MPa at 700 °C to 180 MPa at 800 °C and to 44 MPa at 1000 °C. The decrease in the tensile strength of the hot worked alloy samples with an increase in temperature was much stronger: the UTS decreased from 350 MPa at 600 °C to 91 MPa at 700 °C and to 14 MPa at 1000 °C. The decrease in the tensile strength was accompanied with a noticeable increase in tensile ductility.
5. In the temperature range of 800–1000 °C, the hot worked alloy showed a superplastic-like behavior. The tensile elongation was above 400% and reached 860% at 1000 °C. In spite of void development during tensile deformation in this temperature range, no necks were developed, which is an indirect indication of high strain rate sensitivity of the forged alloy in this temperature range.

Acknowledgement

This work was supported by the Ministry of Science and Education of Russian Federation, grant no. 02.740.11.5184.

References

[1] J.-W. Yeh, S.-K. Chen, S.-J. Lin, J.-Y. Gan, T.-S. Chin, T.-T. Shun, C.-H. Tsau, S.-Y. Chang, Adv. Eng. Mater. 6 (5) (2004) 299–303.
[2] J.-W. Yeh, Ann. Chim.: Sci. Mater. 31 (2006) 633–648.
[3] J.-W. Yeh, Y.-L. Chen, S.-J. Lin, S.-K. Chen, Mater. Sci. Forum 560 (2007) 1–9.
[4] Y.J. Zhou, Y. Zhang, Y.L. Wang, G.L. Chen, Mater. Sci. Eng. A 454–455 (2007) 260–265.
[5] Y.J. Zhou, Y. Zhang, Y.L. Wang, G.L. Chen, Appl. Phys. Lett. 90 (2007) 181904-1–181904-3.
[6] Y.J. Zhou, Y. Zhang, F.J. Wang, Y.L. Wang, G.L. Chen, J. Alloys Compd. 466 (2008) 201–204.
[7] Y.P. Wang, B.S. Li, M.X. ren, C. Yang, H.Z. Fu, Mater. Sci. Eng. A 491 (2008) 154–158.
[8] F.J. Wang, Y. Zhang, Mater. Sci. Eng. A 496 (2008) 214–216.
[9] L.H. Wen, H.C. Kou, J.S. Li, H. Chang, X.Y. Xue, L. Zhou, Intermetallics 17 (2009) 266–269.
[10] C.W. Tsai, M.H. Tsai, J.W. Yeh, C.C. Yang, J. Alloys Compd. 490 (2010) 160–165.
[11] J.M. Zhu, H.M. Fu, H.F. Zhang, A.M. Wang, H. Li, Z.Q. Hu, Mater. Sci. Eng. A 527 (2010) 6975–6979.
[12] O.N. Senkov, G.B. Wilks, J.M. Scott, D.B. Miracle, Intermetallics 19 (2011) 698–706.
[13] O.N. Senkov, J.M. Scott, S.V. Senkova, D.B. Miracle, C.F. Woodward, J. Alloys Compd. 509 (2011) 6043–6048.
[14] C.-W. Tsai, Y.-L. Chen, M.-H. Tsai, J.-W. Yeh, T.-T. Shun, S.-K. Chen, J. Alloys Compd. 486 (2009) 427–435.
[15] O.N. Senkov, G.B. Wilks, D.B. Miracle, C.P. Chuang, P.K. Liaw, Intermetallics 18 (2010) 1758–1765.
[16] K.B. Zang, Z.Y. Fu, J.Y. Zhang, J. Shi, W.M. Wang, H. Wang, Y.C. Wang, Q.J. Zhang, J. Alloys Compd. 502 (2010) 295–299.
[17] T.-T. Shun, Y.-C. Du, J. Alloys Compd. 479 (2009) 157–160.
[18] R.Z. Valiev, I.V. Alexandrov, Bulk Nanostructured Metallic Materials, Akademkniga, Moscow, 2007, p. 398.
[19] G.A. Salishchev, R.M. Imayev, O.N. Senkov, V.M. Imayev, N.K. Gabdullin, M.R. Shagiev, A.V. Kuznetsov, F.H. (Sam) Froes, Mater. Sci. Eng. A 286/2 (2000) 236–243.
[20] G.A. Salishchev, R.I. Imayev, O.N. Senkov, F.H. Froes, JOM 52 (12) (2000) 46–48.
[21] S.V. Zherebtsov, G.A. Salishchev, R.M. Galeyev, O.R. Valiakhmetov, S.Y. Mironov, S.L. Semiatin, Scripta Mater. 51 (2004) 1147–1151.
[22] R.M. Imayev, N.K. Gabdullin, G.A. Salishchev, O.N. Senkov, V.M. Imayev, F.H. Froes, Acta Mater. 47 (1999) 1809–1821.
[23] C.J. Tong, M.R. Chen, S.K. Chen, J.W. Yeh, T.T. Shun, S.J. Lin, S.Y. Chang, Metall. Mater. Trans. A 36A (2005) 1263–1271.
[24] C.J. Tong, Y.L. Chen, S.K. Chen, J.W. Yeh, T.T. Shun, C.H. Tsau, S.J. Lin, S.Y. Chang, Metall. Mater. Trans. A 36A (2005) 881–893.
[25] F.J. Wang, Y. Zhang, G.L. Chen, H.A. Davies, Int. J. Mod. Phys. B 6–7 (2009) 1254–1259.
[26] P. Haasen, Physical Metallurgy, 3rd ed., University Press, Cambridge, UK, 1996.
[27] V.M. Imayev, R.M. Imayev, G.A. Salishchev, Intermetallics 8 (2000) 1–6.
[28] T.G. Nieh, J. Wadsworth, O.D. Sherby, Superplasticity in Metals and Ceramics (Cambridge Solid State Science Series), University Press, Cambridge, UK, 1997.
[29] M.M. Schwartz, New Materials, Processes and Methods Technology, CRC Press, Boca Raton, FL, USA, 2005.